All-printed and stretchable organic electrochemical transistors using a hydrogel electrolyte†

Chi-Hyeong Kim, Mona Azimi, Jiaxin Fan, Harini Nagarajan, Meijing Wang and Fabio Cicoira [ID] *

Stretchable electronic devices are expected to play an important role in wearable electronics. Solution-processable conducting materials are desirable because of their versatile processing. Herein, we report the fabrication of fully stretchable organic electrochemical transistors (OECTs) by printing all components of the device. To achieve the stretchability of the whole body of the devices, a printed planar gate electrode and polyvinyl alcohol (PVA) hydrogel electrolyte were employed. Stretchable silver paste provided a soft feature to drain/source, gate and interconnect, without any additional strategies needed to improve the stretchability of the metallic components. The resulting OECTs showed a performance comparable to inkjet or screen-printed OECTs. The maximum transconductance and on/off ratio were 1.04 ± 0.13 mS and 830, respectively. The device was stable for 50 days and stretched up to 110% tensile strain, which makes it suitable for withstanding the mechanical deformation expected in wearable electronics. This work paves the way for all-printed and stretchable transistors in wearable bioelectronics.

Introduction

Stretchable electronics have gained increasing attention for their great potential in the field of bioelectronics. Stretchability is critical for applications which require intimate contact with curved surfaces or susceptibility to mechanical deformation, such as artificial skin, implantable electronics, and wearable health monitoring devices.[1–3] On-skin wearable electronics should conform to the skin and tolerate mechanical deformations, including bending, twisting, and stretching, with tensile strains of around 30%.[4,5] Stretchable electronics can be achieved mainly by two different approaches: (i) integrating rigid functional devices with stretchable interconnects and (ii) patterning devices with stretchable components.[6,7] Organic semiconducting and conducting polymers have been extensively employed for stretchable electronics owing to their softness, low-temperature processibility, tunable chemical and electrical properties, and, in some cases, ability to be combined with soft and stretchable materials.

Organic electrochemical transistors (OECTs) are widely explored for bioelectronics, due to their low operation voltages (<1 V) and intrinsic signal amplification. Several studies have demonstrated that OECTs are suitable for stretchable bioelectronics.[8–10] An OECT consists of a conducting polymer

channel connected to source and drain electrodes in ionic contact with a gate electrode *via* an ionic medium (liquid or gel). The channel current is modulated by the gate voltage through reversible electrochemical doping/de-doping of the conducting polymer. Poly(3,4-ethylenedioxythiophene)polystyrene sulfonate (PEDOT:PSS) is the most widely used OECT channel material due to its high electrical conductivity, solution processability, and biocompatibility.[11] Although conducting polymers (*e.g.* PEDOT:PSS) can be patterned with photolithography,[12] printing technologies are well-suited for fabricating OECTs, since they permit to pattern the metal contacts and the channel with the same equipment and easily allow to modify the device layout.[13]

For all-printed OECTs, inkjet printing allows the patterning of the components with a relatively high resolution.[14,15] Inkjet printing was employed to fabricate fully printed OECTs with a PEDOT:PSS channel and a graphene gate, used as enzymatic glucose sensors.[16] A water-soluble p-type conjugated polymer, P(DPP-DTT-MS), was inkjet-printed as an active layer of OECTs.[17] Screen printing is faster than inkjet and facilitates mass production.[18] Andersson Ersman *et al.* developed screen-printed PEDOT:PSS based OECTs on flexible substrates for applications in logic circuits, such as NAND gates, multiplexers[19] and inverters operating at relatively high frequencies,[20] and display driver circuits integrated with organic electrochromic displays.[21] Screen-printed OECTs functionalized with enzymes, ion-selective membranes, and bio-recognition elements have also been used as sensors to detect glucose and lactate,[22] ascorbic acid,[23] urea,[24] nutrients in plant sap[25] and

Department of Chemical Engineering, Polytechnique Montréal, Montréal, Québec H3C 3A7, Canada
†Electronic supplementary information (ESI) available. See DOI: https://doi.org/10.1039/d2nr06731e

DNA.[26] Although several flexible OECTs have been fabricated by printing technologies, only a few studies on printed stretchable OECTs have been reported.

For applications requiring a longer device operation, aqueous electrolytes, commonly used for gating OECTs, can be replaced by printable gels containing ions.[27–30] Such gels may also provide a soft interface between electronic devices and biological systems, which improves contact and adhesion on tissues.[31,32] OECTs based on gel electrolytes have been employed for logic circuits, which can be integrated with biosensors to process detected signals.[33] In addition, a gel electrolyte functionalized with bio-receptors has been used for biosensing.[24] Two main classes of gel electrolytes are commonly used in OECTs: ion gels and hydrogels. Ion gels consist of an ionic immobilized into a polymeric matrix. Since the ion gels are mechanically bendable and thermally stable, they are suitable for flexible electronics. Bischak et al. utilized an ion gel as an ion exchange layer and used a flexible OECT to sense action potential in a flytrap plant.[34] Gao et al. reported synaptic plasticity of ion gel gated OECTs[35] and their long-term synaptic behavior.[36] Ion gels are not generally biocompatible, especially imidazolium-based ones, which prevents their use in bioelectronics,[37,38] whereas biocompatible hydrogel can be fabricated from a wide range of naturally sourced, bioinspired and biocompatible materials.[39] Hydrogel also show tissue-like mechanical properties,[40] with Young's moduli ranging from 1 Pa to 300 MPa, covering the typical values for skin and muscles (200–500 kPa), brain tissue, and spinal cords (500 Pa–200 kPa).[41] Such mechanical properties minimize the mechanical mismatch with soft tissues, making hydrogels ideal candidates for implants and wearable bioelectronics. Recently, Wang et al. developed stretchable all-polymer OECTs based on biocompatible gelatin hydrogels working as neuromorphic devices and glucose sensors.[39] Jo et al. showed that gelatin electrolyte-based OECTs can be used for pH-modulated electrochemical logic circuits.[42] Ko et al. demonstrated self-healing OECTs by introducing poly(vinyl alcohol) hydrogel to the active channel material.[43] Liu et al. reported OECTs with a dual network anti-freezing hydrogel composed of crosslinked polyacrylamide and carrageenan,[44,45] able to operate at −30 °C. They also studied the neuromorphic behavior and transient response of the devices. However, the use of hydrogel electrolytes applied to stretchable OECTs remains largely unexplored. This is likely because inkjet and screen printing are not suitable to print hydrogels, as they require inks within specific viscosity ranges (i.e., inkjet printers require low viscosity, whereas screen printers require high viscosity). Therefore, even when the channel end the electrodes of the OECTs are printed, hydrogel electrolytes are typically casted or manually attached on the devices.[43,46]

In this study, we fabricated all-printed and stretchable OECTs on stretchable thermoplastic polyurethane (TPU), using a printed circuit board (PCB) printer. Devices gated with hydrogels exhibited performance similar those gated with aqueous gating media and were operated up to 50 days, maintaining the transconductance at around 60% of its initial value. The devices show a stretchability of ~60% along the channel direction and of ~150% in the perpendicular direction. This study contributes to the improvement of long-term stability and stretchable characteristics of OECTs, with possible applications in printed biosensors.

Experimental details

Materials

PEDOT:PSS screen-printing ink (Clevios SV3 STAB, Heraeus, Germany) was purchased from Heraeus (700 Ohm sq^{-1} sheet resistance declared by the supplier). According to the data supplied by the company, the ink contains a significant amount of propane-1,2-diol, 2-2′-oxydiethanol and other additives in lower concentrations. Screen-printing thermoplastic silver (Ag) ink (Ag paste 520 EI) was donated by Chimet S.p.A (Italy). Thermoplastic polyurethane (TPU) on removable silicon paper (Elecrom Stretch White, thickness of 80 μm) was purchased from Policrom Screens (Italy). A silicone elastomer kit (SYLGARD® 184), used to prepare polydimethylsiloxane (PDMS), was purchased from Dow Corning. Polyvinyl alcohol (PVA, M_w 89–98 kDa) and NaCl (≥99.5%) were purchased from Sigma-Aldrich. Dimethyl sulfoxide (DMSO) and glycerol were purchased from Caledon Ltd. Sodium hypochlorite (NaClO) solution (5% w/v) was purchased from LabChem, Inc. Ag/AgCl (E202) pellet electrode was purchased from Warner Instruments.

Preparation and characterization of hydrogel gating media

Three types of PVA-based hydrogels containing NaCl (Table 1) were used as the gating media and were either printed or manually placed on the transistor channel. PVA (13 wt%) was dissolved in a 0.1 M NaCl aqueous solution (PVA hydrogels) at 85 °C under vigorous stirring. As drying over time of hydrogels may hinder the long-term stable operation of OECTs,[47] we prepared hydrogels using mixtures of water with DMSO (normal boiling point 189 °C) and glycerol (normal boiling point 290 °C), which are known to raise the water boiling point.[39,48] To prepare these gels, 13% PVA and the equivalent of 0.1 M NaCl were dissolved in water mixed with 30 v/v%, DMSO (hydrogel named D_PVA) and 45 v/v% glycerol (named G_PVA) at 85 °C under vigorous stirring. The amounts of DMSO and glycerol were selected because they yielded a mechanically stable hydrogel.

Physical crosslinking of PVA hydrogel was achieved with a freezing and thawing process, by drop-casting the precursor solution on a Petri dish, freezing at −15 °C for 12 hours, and thawing at room temperature.[49]

Table 1 Composition and names of the hydrogel electrolytes used in this work

Hydrogel	PVA (wt%)	H$_2$O (v/v%)	Glycerol (v/v%)	DMSO (v/v%)
PVA	13	100	0	0
G_PVA	13	55	45	0
D_PVA	13	70	0	30

Electrochemical impedance spectroscopy (EIS) of hydrogel electrolytes was carried out in a Swagelok cell (Beyond Battery) with a VERSASTAT 4 (Princeton Applied Research) potentiostat. The drop-casted hydrogel electrolytes (2 mm thickness) were cut in round shapes and loaded between stainless steel electrodes in a Teflon™ body (inner diameter: 13 mm). EIS was carried out with AC voltage of 10 mV in frequency range 10^5–10^{-1} Hz. The ionic conductivity (σ) which was calculated with the following equation:

$$\sigma = \frac{d}{R_b S} \qquad (1)$$

where d is the thickness of the hydrogel, S is the contact area between the hydrogel and the electrode of the cell, R_b is the bulk resistance, which is equal to the value of the real impedance in the high frequency region ($>10^3$ Hz).

The mechanical tensile properties of hydrogels were measured using a mechanical tester (Mach-1 v500csst, Biomomentum Inc., Canada). Samples in dog-bone shapes (~1 mm thickness, ~3.2 mm width, ~15 mm length) were stretched at 0.3 mm s^{-1} strain rate.

OECT fabrication

OECTs were patterned on the stretchable TPU substrates with a PCB printer (Voltera V-One), already used by our group to pattern devices on flexible polyethylene terephthalate.[50] The TPU substrates were cleaned with deionized water (DIW), dried using an air-blowing gun and attached to a glass slide (Corning®) with double-sided tape (3 M) to facilitate handling. The stretchable Ag ink, used to pattern gate, source and drain electrodes, was homogenized in a sonicator (CPX2800, Fisherbrand™) for 15 min before use. The Ag/AgCl gate was obtained by patterning the gate electrode, baking at 120 °C for 20 min on a hotplate (Corning®), and bleaching with a 5% NaClO solution for 1 hour. The Ag source and drain electrodes were then patterned next to the Ag/AgCl gate and baked at 120 °C for 20 minutes. The PEDOT:PSS ink was homogenized in the sonicator and filtered using a syringe filter (CHROMSPEC UV Syringe Filters, 5.0 μm pore size) before printing. PEDOT:PSS channels were printed between the source and drain electrodes (channel dimensions: width W = ~1 mm, length L = ~1.5 mm, thickness d = ~1 μm) and baked at 120 °C for 30 min. PDMS (silicone elastomer with a curing agent at a ratio of 10 : 1, mixed for 3 min at 2000 rpm in a centrifugal mixer) was printed over the Ag electrodes and then cured at 120 °C for 30 min on a hotplate. This step is necessary to prevent faradaic reactions between the Ag electrodes and the electrolyte. The hydrogel ink was printed on the top of the channel and the gate electrode (Fig. 1a). To achieve cross-linking of the hydrogels, the devices were kept in freezer at −15 °C for 12 hours and thawed at room temperature. To prepare hydrogel electrolytes manually placed on OECTs, the hydrogel inks were drop-casted and gelled by the freezing and thawing process described above. The gel electrolyte solidified on the Petri dish was cut into rectangles (~1.5 × 1.5 cm^2) and placed on the printed devices.

The thickness of the electrodes and the PEDOT:PSS channels were derived from the cross-section images of field-emission scanning electron microscopy (FE-SEM, JEOL, JSM-7500F).

Device characterization

Electrical measurements were performed using an Agilent B1500A source/measure unit (SMU) under ambient conditions. For transfer characteristics (I_D–V_G), the drain current (I_D) was recorded at a fixed drain–source voltage (V_D) of −0.4 V, while the gate voltage (V_G) was swept from −0.6 V to 1 V. To obtain the output characteristics (I_D–V_D), V_D was gradually changed from 0 V to −0.8 V, while V_G was varied from −0.6 V to 0.8 V in 0.2 V steps for every V_D sweep. The I–V characterizations were performed at a scan rate of 20 mV s^{-1}, and the data points were recorded for every 0.01 V step. The transconductance (g_m = $\Delta I_D/\Delta V_G$) of the OECTs was extracted from their transfer curves. Normalized g_m values were obtained by dividing g_m by dimension factors Wd/L.

The switching response of the OECTs was measured using a PXIe-4141 source/measurement unit controlled by LabVIEW software. A gate voltage pulse (ΔV_G = 0.7 V) was applied for 30 s, followed by a 0 V bias maintained for a relaxation time of 80 s while keeping V_D = −0.4 V. For the operational stability test, 500 cycles at 0.4 V gate pulse for 20 s and 0 V for 30 s were done while applying a V_D of −0.4 V.

Electromechanical characterization

The electromechanical properties of the printed stretchable Ag electrodes (15 mm × 1 mm) on TPU were measured using a mechanical tester (Mach-1 v500csst, Biomomentum Inc., Canada) coupled with a Keysight B2902A SMU. The Ag electrodes were stretched parallel to their long direction at a rate of 10% per second.

Stretchable OECTs (channel dimensions of $W = L$ = 8 mm) were measured using a LabVIEW-controlled homemade tensile tester coupled with an Agilent B2900A SMU. In the cyclic strain test, the OECTs were repeatedly stretched and released 1000 times at 30% strain at a rate of 0.2 mm s^{-1}.

Results and discussion

Fabrication of all-printed and stretchable OECTs

The process flow for OECT fabrication is shown in Fig. 1a and microscopic image of a printed stretchable OECT is shown in Fig. 1b. The electrodes were printed using a stretchable Ag ink formulation, instead of using strategies to make rigid electrodes stretchable, such as pre-stretching[51,52] or 3D-wavy structures on soft substrates.[10,53] The Ag electrodes exhibited good stretchability (Fig. S1a†), with no significant failures observed below ~250% strain (Fig. S1b†). The resistance of the Ag lines increased ~10 times at ~30% strain and remained stable during stretch-release cycles from 0% and 30% (Fig. S1c†). The electrodes show a thickness of ~20 μm, which, in the case of the gate, includes a ~5 μm AgCl layer (Fig. S2a†). The thickness of the PEDOT:PSS channel is ~1 μm (Fig. S2b†). The
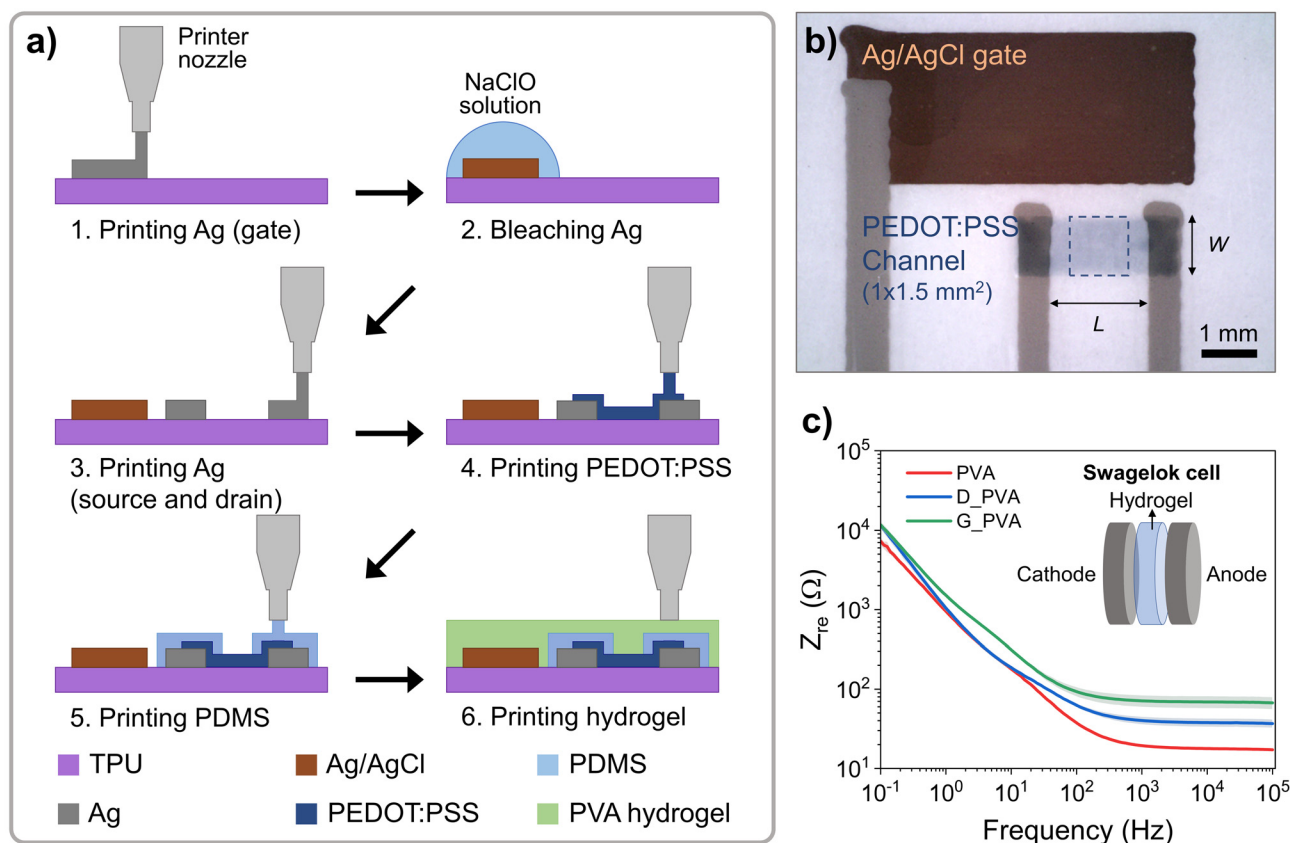
Fig. 1 (a) Process flow to fabricate the printed OECTs. Step 1: printing stretchable Ag paste as gate electrode on TPU substrate. Step 2: bleaching the printed Ag with NaClO solution to form Ag/AgCl on the surface (thickness ~20 μm including a ~5 μm AgCl layer). Step 3: printing the Ag source, drain, and interconnects (thickness ~20 μm). Step 4: printing of the PEDOT:PSS channel (thickness ~1 μm). Step 5: printing PDMS to cover source, drain, gate interconnects and the overlap region of PEDOT:PSS with Ag. Step 6: printing hydrogel electrolytes over the gate and channel. (b) Microscopic image of the device. The dashed area indicates the area of the channel (1 × 1 mm^2), which is not covered by PDMS. (c) Electrochemical impedance (Z_{re}) of the PVA-based hydrogel electrolytes from 10^5 to 10^{-1} Hz, using Swagelok cell. The solid lines are the average values measured from 3 different samples and the shaded area shows the error bars, which represent standard deviation. Since the standard deviation is very small, the shaded area is imperceptible in the graph.

D_PVA and G_PVA hydrogel electrolytes were stretchable up to ~500% strain and showed Young's moduli of ~190 kPa and ~350 kPa, respectively (Fig. S3†). These mechanical properties are suitable for application in stretchable OECTs.

Electrochemical impedance spectroscopy (EIS) was carried out to evaluate the ionic conductivity of the hydrogels (Fig. 1c). The hydrogels show similar impedance in the low frequency range (<10 Hz). In the high frequency range (>10^3 Hz), D_PVA (~40 ohms) and G_PVA (~70 ohms) showed higher impedances than PVA (~20 ohms). This means that, D_PVA (~5 S cm^{-1}) and G_PVA (~3 S cm^{-1}) possess low ionic conductivities with respect to PVA (~10 S cm^{-1}). This behaviour is likely caused by intermolecular interactions between the glycerol or DMSO molecules and hydrated ions. Both glycerol and DMSO have hydroxyl groups, potentially interacting with hydrated cations through hydrogen bonding and electrostatic forces, interfering with the ion transport in the hydrogel electrolyte.[54,55] It can be expected that these electrochemical properties have an effect on the transient behaviour of the OECTs.

OECT *I–V* characteristics

All printed OECTs exhibited p-type depletion mode operation, as expected for PEDOT:PSS.

The figures of merit of the OECTs using the four types of electrolytes are summarized in Table 2. The transfer characteristics (I_D–V_G) obtained from the average of four devices for each electrolyte (Fig. 2a), and the output characteristics (Fig. 2b and Fig. S4†) reveal that hydrogel-gated OECTs show comparable performance to those using an aqueous electrolyte gated with a pellet Ag/AgCl electrode (Fig. S5†). Devices with printed and manually attached PVA hydrogels show very similar characteristics (Fig. S6†). These results prove that our printing technology allows rapid patterning of devices with state-of-the-art characteristics. The backward sweeps of the transfer curves show similar hysteresis characteristics regardless of the electrolyte (Fig. S7†). For all devices the maximum transconductance (g_m) is ~1 mS (at V_G = 0.1). The output current show similar values at the same applied voltages and

Table 2 Figures of merits of all-printed OECTs. The average values in this work were calculated from the results of 4 different samples for each type of electrolyte. Error values represent standard deviation. Dimensionally normalized g_m in this work and other references was calculated from the transconductance and the channel dimension (Wd/L) given in the references

Printing method	Channel material	Electrolyte	$W/L/d$ (μm)	On/off ratio	g_m (mS)	Dimensionally normalized g_m (S cm^{-1})	Time constant τ (ms)	Ref.
PCB (direct-ink write)	PEDOT:PSS	NaCl solution	1000/1000/1	350 ± 30	1.2 ± 0.1	17.4 ± 1.7	14.5 ± 2.7	This work
		PVA		150 ± 10	0.9 ± 0.1	12.8 ± 1.4	20.7 ± 3.5	
		D_PVA		280 ± 20	0.8 ± 0.1	11.6 ± 1.0	41.8 ± 8.0	
		G_PVA		830 ± 80	1.0 ± 0.1	15.6 ± 1.9	156.4 ± 26.0	
Inkjet	PEDOT:PSS	Cellulose-lithium-Based hydrogel	1000/500/0.208	46	0.06	5.77	N/A	64
	P(DPP-PTT-MS)-PE cleaved	PVDF-HFP/[EMIM][TFSI]	2000/200/0.05	N/A	0.8	2.2	N/A	17
	PEDOT:PSS	PBS solution	1000/3000/1	N/A	~1	30	N/A	16
	PEDOT:PSS	PEO$_{25}$/LiTFSI	2000/3000/N/A	175	1.67	N/A	N/A	65
Screen	PEDOT:PSS	PBS solution	2000/3000/0.28	N/A	0.004	0.21	N/A	26
	PEDOT:PSS	KCl solution	700/700/2.5	N/A	5	20	N/A	25
	PEDOT:PSS	Chitosan-based sol–gel	500/5000/0.5	N/A	0.017	3.4	N/A	22
3D	PEDOT:PSS	NaCl solution	953/417/9	775	43.32	20.91	N/A	66
	PEDOT:PSS	NaCl solution	178/118/7.1	1330	31.8	27.99	N/A	67

the threshold voltages are ∼0.6 V. The capacitance and the charge carrier mobility of the semiconducting channel and applied gate potential between the electrolyte and the channel mainly contribute to the steady state performance of OECTs. Therefore, it is expected that devices with the same channel, gate electrode and electrolyte ion concentration show similar behavior. The negligible difference in the I–V characteristics of the OECTs may be attributed to the influence of freezing-thawing process or anti-drying agents in the hydrogel electrolytes.

To long-term stability of the G_PVA and D_PVA devices was evaluated by measuring the devices consecutively for several days after fabrication and storage under ambient conditions. Devices using G_PVA as a gating medium worked until the 50th day. The I_D at V_G = −0.6 V decreased from ∼0.6 mA to ∼0.3 mA after 40 days and then remained stable until the 50th day (Fig. 2c). The transconductance (g_m) converged to about 60% of its initial value on the 50th day (Fig. 2e). For the D_PVA OECT (Fig. 2d), the on-current gradually decreased until the hydrogel was dehydrated and partially delaminated on the 21st day, and completely dried on the 24th day. As shown by the data above, the device degradation over time mostly depends on drying of the hydrogels, although smaller contributions from the degradation of PEDOT:PSS cannot be totally excluded.

Transient behavior of the OECTs

To investigate the switching speed of OECTs, we measured the OECT transient responses (Fig. 3a and S8†). It is worth noticing that the ON–OFF (dedoping) is faster than the OFF–ON (doping) response. This behavior may be attributed to the slow migration of the cations trapped in the PEDOT:PSS films below the protective PDMS layer (Fig. S9a†) when the device is

on the OFF state. This assumption is supported by the faster OFF–ON switching in absence of the PDMS protective layer (Fig. S9b†). Therefore, we analyzed the ON–OFF response to study the switching properties of the devices. The 4th spike was selected to allow pre-conditioning of the devices and fitted using an exponential decay model to extract the time constants. Since the monolithic decay model was unfitted with the measured I_D, a triple exponential decay model was employed, based on the following equation:[56]

$$I_D(t) = I_0 - I_1 \exp\left(-\frac{t}{\tau_1}\right) - I_2 \exp\left(-\frac{t}{\tau_2}\right) - I_3 \exp\left(-\frac{t}{\tau_3}\right) \quad (2)$$

where t is time, and I_0 is the initial drain current. I_1, I_2, and I_3 are the current coefficients for fitting. τ_1, τ_2, and τ_3 are the time constants for the dedoping process (results of the fitting shown in Fig. 3b). The triple exponential decay of the drain current may be ascribed to different ion and charge carrier transport contributions within the device, such as de-doping the channel under the applied gate bias, holes transport within the channel between source and drain, and the delayed re-doping due to PDMS insulator overlapping with the PEDOT:PSS layer. A correlation of the exact mechanism with each specific time constant and current coefficient would require more extensive studies. The weight averages of the time constants for all four types of OECTs were calculated with the following equation:[57]

$$\tau = \frac{I_1\tau_1 + I_2\tau_2 + I_3\tau_3}{I_1 + I_2 + I_3}. \quad (3)$$

The results of the arithmetic mean time constants acquired from three different devices for each electrolyte type are reported in Table 2. The time constants indicate the speed of de-doping process in the channel. The fastest dedoping occurs in devices using aqueous electrolytes. A higher time constant
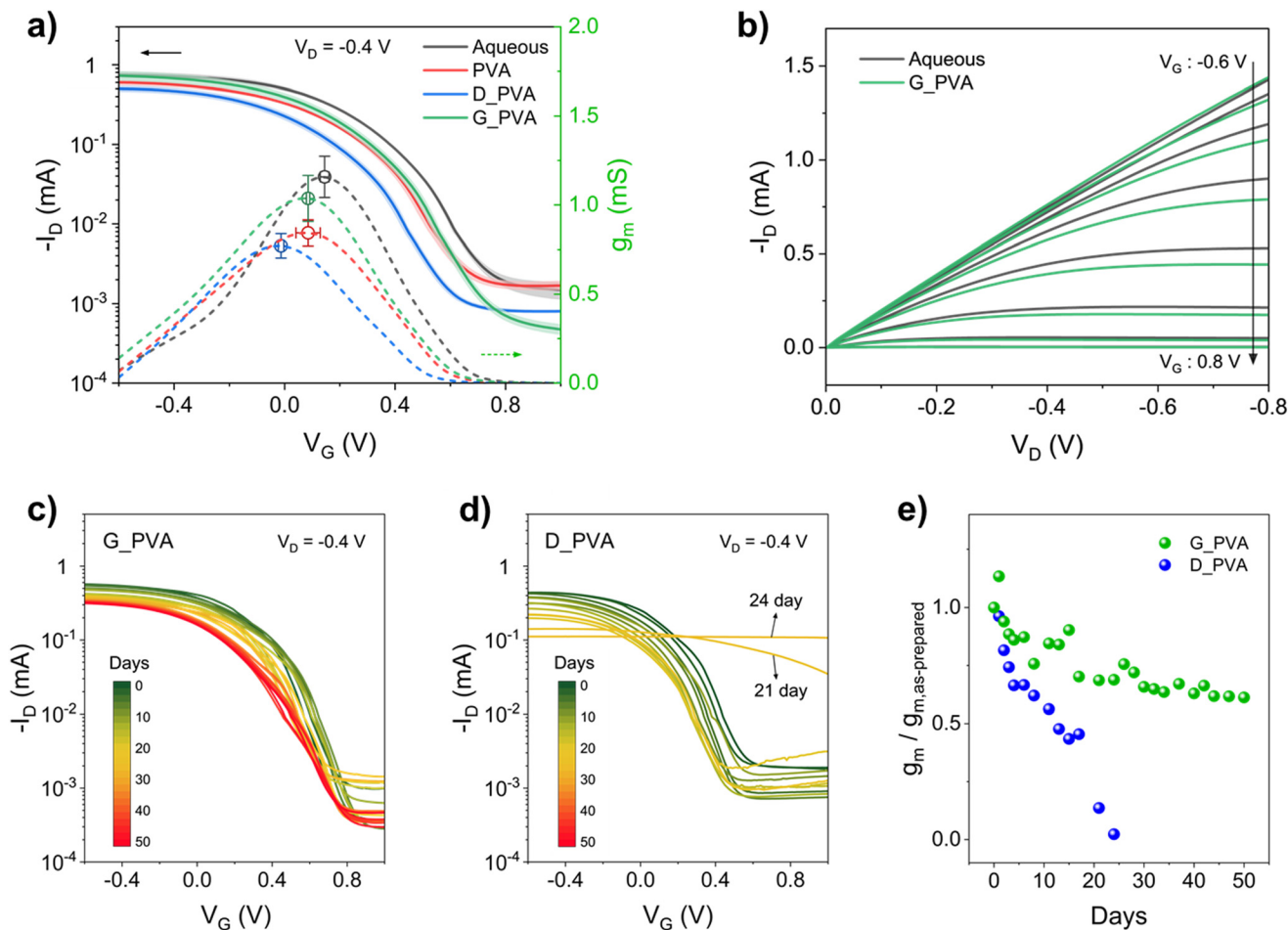
Fig. 2 OECT current–voltage characteristics. (a) Transfer (solid line) and transconductance (dashed line) curves with 4 types of electrolytes; NaCl 0.1 M aqueous solution (black), PVA hydrogel (red), D_PVA (blue), and G_PVA (green). The solid curves represent the mean values of four device measurements for each electrolyte and the shaded areas indicate the error. The points at each maximum transconductance are plotted with error bars, which represents standard deviation. (b) Output curves obtained with aqueous electrolyte and G_PVA. Long-term stability tests of (c) D_PVA and (d) G_PVA hydrogel-based OECTs. (e) The ratio of transconductances extracted from (c) and (d) with respect to the g_m of as prepared (day 0) OECT. (Blue circle: D_PVA, green circle: G_PVA). For transfer characteristics (I_D–V_G), the drain current (I_D) was recorded at a fixed drain–source voltage (V_D) of −0.4 V, while the gate voltage (V_G) was swept from −0.6 V to 1 V. To obtain the output characteristics (I_D–V_D), V_D was gradually changed from 0 V to −0.8 V, while V_G was varied from −0.6 V to 0.8 V in 0.2 V steps for every V_D sweep.

is found for PVA OECTs, likely due hindered transport of hydrated cations due to an increase in ionic resistance.[58] The D_PVA and G_PVA OECTs showed larger time constants. This behaviour is consistent with the smaller ionic conductivity of D_PVA (∼5 S cm^{-1}) and G_PVA (∼3 S cm^{-1}) with respect to PVA (∼10 S cm^{-1}), which may be caused by the intermolecular interaction between hydrated ions and DMSO or glycerol. In the transient behaviour of OECTs, the drain current can be characterized with ion and hole (or electron) transit time.[59] In our case, hole transport in the PEDOT:PSS layer is expected to be nearly the same since the OECTs have the same channel material. The current based on ion transport in the electrolytes dominantly influences the difference between the time constants of the electrolytes. Ion mobility and ion concentration mainly contribute to Ionic conductivity.[60] Since the ion concentration in the hydrogel electrolytes is the same, the smaller ionic conductivity of the D_PVA and G_PVA likely leads to

slower ion transport and larger ion transit time, which reflects the value of the time constants found for our OECTs of OECTs. Therefore, G_PVA based OECTs show characteristics that are more suitable for applications that do not require rapid monitoring.

The operational stability test of the G_PVA OECTs was performed with trains of gate-potential pulses for 7 h (Fig. 3c). Although the ON current during the last cycles decreased by ∼50% compared to the initial value, the average ON/OFF ratio for the last five cycles increased only of about 10% with respect to the first five cycles. This indicates that G_ PVA OECTs are capable of continuous operation over a long period.

OECT operation under strain

To evaluate the stretchability of the printed OECTs and their stability under strain, bi-axial electromechanical tests were conducted using G_PVA OECTs, as they exhibit the most stable
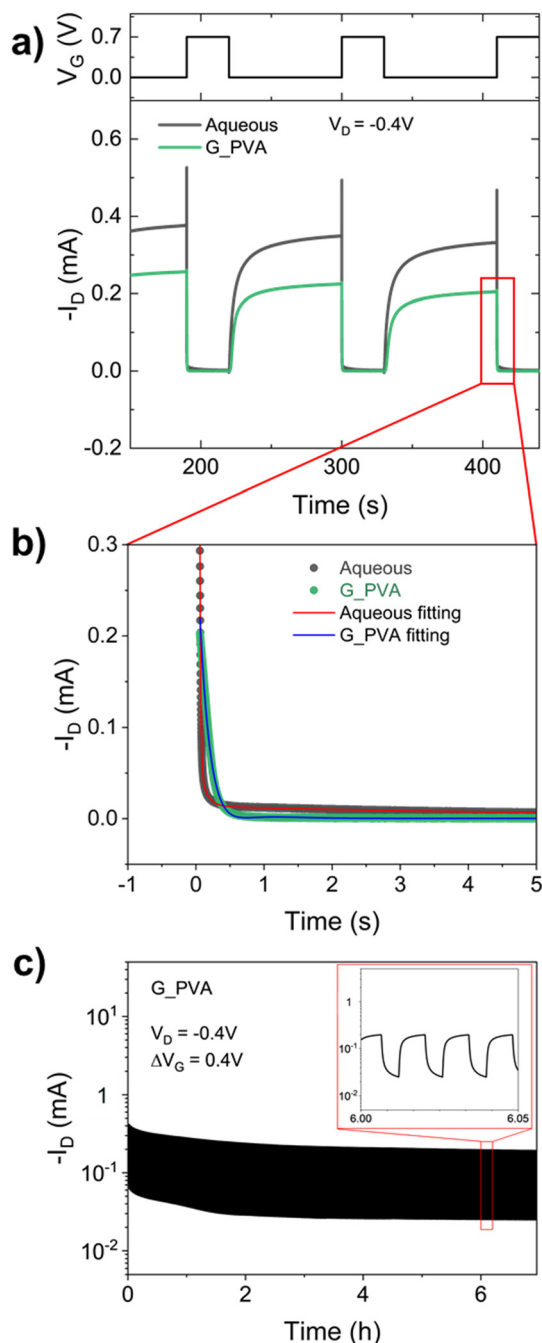
Fig. 3 Transient response of OECTs. (a) Source–drain current spikes of aqueous and G_PVA electrolytes. A 0.7 V gate pulse was applied for 30 s and 0 V bias was maintained for 80 s as the relaxation time. (b) Fitting with triple decay exponential model. (c) Operational stability test of G_PVA with 500 cycles of between 0 V and 0.4 V gate potential pulse for 20 s and relaxing time for 30 s. The inset is a magnified plot from 6 h for 3 min.
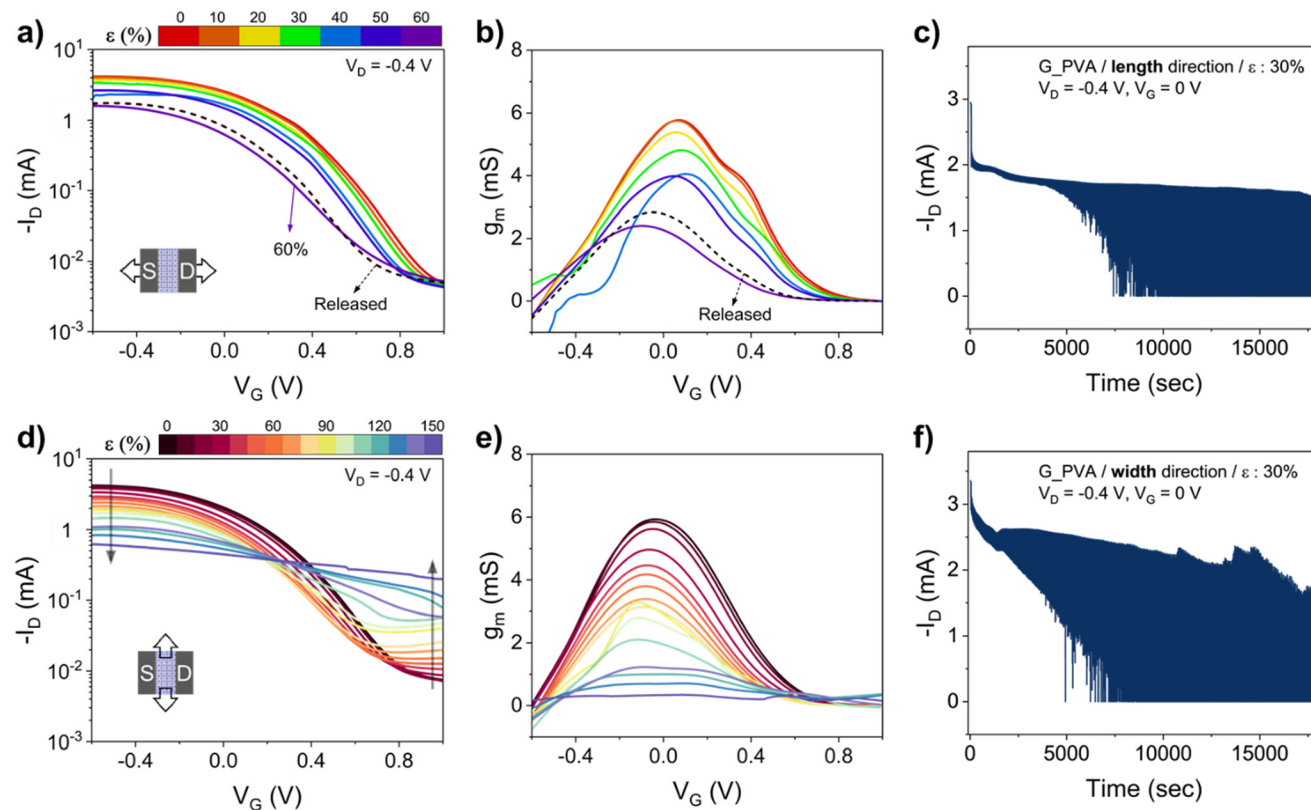
long-term performance. When stretched by 10% increments in the length direction of the PEDOT:PSS channel (parallel strain, Fig. 4a and b), the OECTs can withstand strains up to 60%. As the OECT was stretched to 50%, the ON current and the maximum g_m gradually decreased to ~60% and ~70% of

their initial values, respectively. The two values at 60% strain further decreased to ~20% and ~40%. The ON/OFF ratio of the stretched OECT remained ~100 up to 50% strain. The electrical connection of the device was interrupted at 70% strain, and cracks in the width direction of the channel were found on the PEDOT:PSS film (Fig. S10†). The device released from 70% to 0% strain showed the same performance as the 60% stretched OECT (dashed line in Fig. 4b). When the device was released, the physical contact of the cracked PEDOT:PSS films led to the recovery in the electrical connection. Applying the strain in the width direction of the PEDOT:PSS channel strains (perpendicular strain, Fig. 4d and e), led to a decrease of the ON current and an increase of the OFF current. At approximately 120% strain, the g_m decreased significantly. The ON/OFF ratio of the OECT was reduced below 10^2 while stretching more than 70% and decrease to less than 10 under 120%. The cracks in the PEDOT:PSS film were in this case parallel to the channel. Overall, our results show that the OECTs are sufficiently strain-insensitive up to 50% for parallel and up to 100% for perpendicular strain. These properties are very promising for applications in wearable and on-skin electronics.[4]

Our group previously reported stretchable OECTs obtained *via* several strategies. Devices with stretchability as high as 30% were achieved *via* the pre-stretched method.[51] Strain-insensitive OECTs up to 30% strain were achieved by controlling the thickness and baking temperature of the active channel.[61] Introduction of polyethylene glycol to channel enhanced the stretchability of the OECTs to 45% strain.[62] Fabrication of sub-micro fibrous structure of the channel by electrospinning resulted in the stretchable devices as 50% strain.[63] In this work, we further improved the stretchability of OECTs up to 60%.

These values are in line with findings of other research groups. OECTs on the biomimicking-buckled substrate achieved omnidirectional stretchability up to 30%.[10] OECTs fabricated by combining the pre-stretching method and engineering the topography of the substrate showed 30% stretchability.[53] OECT arrays on a honeycomb grid substrate stably performed under 15% tensile strain.[9] Integration of 100% pre-stretching and honeycomb structure of the channel exhibited the high stretchability of the OECTs up to 100%.[52] Anther OECT also achieved stability in 100% tensile strain using a 3D-microstructured channel, serpentine organic material interconnects, and an additive for the active channel.[39]

Multiple-cycle stretchability tests were performed at a 30% cyclic strain (Fig. 4c and f). A drop in the drain current was observed after a few initial strain cycles, and the current slightly decreased until approximately 7000 s in the length direction and approximately 5000 s in the width direction. The initial changes in the drain current are consistent with the resistance change of stretched PEDOT:PSS films in our previous work.[50] The sudden current changes after 5000 s, are likely related to the stretchable Ag interconnects. According to the magnified plot of the multiple-cycle stretchability tests (Fig. S11†), the current spiked every time the OECTs were stretched and released. In our previous work, a similar test at

uted to the preparation of hydrogels and helped with experiments. Fabio Cicoira supervised this project. Chi-hyeong Kim, Mona Azimi, Jiaxin Fan, Meijing Wang, and Fabio Cicoira supervised experimental work and data analysis, discussed the results and edited the manuscript.

Conflicts of interest

The authors declare that they have no conflicts of interest.

Acknowledgements

References

1 X. Fan, W. Nie, H. Tsai, N. Wang, H. Huang, Y. Cheng, R. Wen, L. Ma, F. Yan and Y. Xia, *Adv. Sci.*, 2019, **6**, 1900813.

2 M. Wang, Y. Luo, T. Wang, C. Wan, L. Pan, S. Pan, K. He, A. Neo and X. Chen, *Adv. Mater.*, 2021, **33**, 2003014.

3 T. Q. Trung and N. E. Lee, *Adv. Mater.*, 2016, **28**, 4338–4372.

4 D. H. Kim, N. Lu, R. Ma, Y. S. Kim, R. H. Kim, S. Wang, J. Wu, S. M. Won, H. Tao, A. Islam, K. J. Yu, T. I. Kim, R. Chowdhury, M. Ying, L. Xu, M. Li, H. J. Chung, H. Keum, M. McCormick, P. Liu, Y. W. Zhang, F. G. Omenetto, Y. Huang, T. Coleman and J. A. Rogers, *Science*, 2011, **333**, 838–843.

5 J. Zhao, Z. Chi, Z. Yang, X. Chen, M. S. Arnold, Y. Zhang, J. Xu, Z. Chi and M. P. Aldred, *Nanoscale*, 2018, **10**, 5764–5792.

6 Y. Wang, C. Zhu, R. Pfattner, H. Yan, L. Jin, S. Chen, F. Molina-Lopez, F. Lissel, J. Liu, N. I. Rabiah, Z. Chen, J. W. Chung, C. Linder, M. F. Toney, B. Murmann and Z. Bao, *Sci. Adv.*, 2017, **3**, 1602076.

7 S. Wang, J. Xu, W. Wang, G. N. Wang, R. Rastak, F. Molina-Lopez, J. W. Chung, S. Niu, V. R. Feig, J. Lopez, T. Lei, S. K. Kwon, Y. Kim, A. M. Foudeh, A. Ehrlich, A. Gasperini, Y. Yun, B. Murmann, J. B. Tok and Z. Bao, *Nature*, 2018, **555**, 83–88.

8 Y. Dai, S. Dai, N. Li, Y. Li, M. Moser, J. Strzalka, A. Prominski, Y. Liu, Q. Zhang, S. Li, H. Hu, W. Liu, S. Chatterji, P. Cheng, B. Tian, I. McCulloch, J. Xu and S. Wang, *Adv. Mater.*, 2022, **34**, 2201178.

9 W. Lee, S. Kobayashi, M. Nagase, Y. Jimbo, I. Saito, Y. Inoue, T. Yambe, M. Sekino, G. G. Malliaras, T. Yokota, M. Tanaka and T. Someya, *Sci. Adv.*, 2018, **4**, aau2426.

10 Y. Li, N. Wang, A. Yang, H. Ling and F. Yan, *Adv. Electron. Mater.*, 2019, **5**, 1900566.

11 S.-M. Kim, N. Kim, Y. Kim, M.-S. Baik, M. Yoo, D. Kim, W.-J. Lee, D.-H. Kang, S. Kim, K. Lee and M.-H. Yoon, *NPG Asia Mater.*, 2018, **10**, 255–265.

12 S. Zhang, E. Hubis, C. Girard, P. Kumar, J. DeFranco and F. Cicoira, *J. Mater. Chem. C*, 2016, **4**, 1382–1385.

13 X. Du, S. P. Wankhede, S. Prasad, A. Shehri, J. Morse and N. Lakal, *J. Mater. Chem. C*, 2022, **10**, 14091–14115.

14 F. A. Viola, J. Barsotti, F. Melloni, G. Lanzani, Y. H. Kim, V. Mattoli and M. Caironi, *Nat. Commun.*, 2021, **12**, 5842.

15 F. Molina-Lopez, T. Z. Gao, U. Kraft, C. Zhu, T. Ohlund, R. Pfattner, V. R. Feig, Y. Kim, S. Wang, Y. Yun and Z. Bao, *Nat. Commun.*, 2019, **10**, 2676.

16 S. Demuru, C.-H. Huang, K. Parvez, R. Worsley, G. Mattana, B. Piro, V. Noël, C. Casiraghi and D. Briand, *ACS Appl. Nano Mater.*, 2022, **5**, 1664–1673.

17 B. Schmatz, A. W. Lang and J. R. Reynolds, *Adv. Funct. Mater.*, 2019, **29**, 1905266.

18 M. Zabihipour, R. Lassnig, J. Strandberg, M. Berggren, S. Fabiano, I. Engquist and P. Andersson Ersman, *npj Flexible Electron.*, 2020, **4**, 15.

19 P. Andersson Ersman, D. Westerberg, D. Tu, M. Nilsson, J. Åhlin, A. Eveborn, A. Lagerlöf, D. Nilsson, M. Sandberg, P. Norberg, M. Berggren, R. Forchheimer and G. Gustafsson, *Flexible Printed Electron.*, 2017, **2**, 045008.

20 M. Zabihipour, D. Tu, J. Strandberg, M. Berggren, I. Engquist and P. Andersson Ersman, *Adv. Mater. Technol.*, 2021, **6**, 2100555.

21 P. Andersson Ersman, M. Zabihipour, D. Tu, R. Lassnig, J. Strandberg, J. Åhlin, M. Nilsson, D. Westerberg, G. Gustafsson, M. Berggren, R. Forchheimer and S. Fabiano, *Flexible Printed Electron.*, 2020, **5**, 024001.

22 G. Scheiblin, A. Aliane, X. Strakosas, V. F. Curto, R. Coppard, G. Marchand, R. M. Owens, P. Mailley and G. G. Malliaras, *MRS Commun.*, 2015, **5**, 507–511.

23 L. Contat-Rodrigo, C. Pérez-Fuster, J. V. Lidón-Roger, A. Bonfiglio and E. García-Breijo, *Org. Electron.*, 2017, **45**, 89–96.

24 M. Berto, C. Diacci, L. Theuer, M. Di Lauro, D. T. Simon, M. Berggren, F. Biscarini, V. Beni and C. A. Bortolotti, *Flexible Printed Electron.*, 2018, **3**, 024001.

25 E. J. Strand, E. Bihar, S. M. Gleason, S. Han, S. W. Schreiber, M. N. Renny, G. G. Malliaras, R. R. McLeod and G. L. Whiting, *Adv. Electron. Mater.*, 2022, **8**, 2100853.

26 M. Sensi, G. Migatti, V. Beni, T. M. D'Alvise, T. Weil, M. Berto, P. Greco, C. Imbriano, F. Biscarini and C. A. Bortolotti, *Macromol. Mater. Eng.*, 2022, **307**, 2100880.

27 J. H. Cho, J. Lee, Y. Xia, B. Kim, Y. He, M. J. Renn, T. P. Lodge and C. D. Frisbie, *Nat. Mater.*, 2008, **7**, 900–906.

28 Y. Xia, J. Cho, B. Paulsen, C. D. Frisbie and M. J. Renn, *Appl. Phys. Lett.*, 2009, **94**, 013304.

29 D. Song, F. Zare Bidoky, E. B. Secor, M. C. Hersam and C. D. Frisbie, *ACS Appl. Mater. Interfaces*, 2019, **11**, 9947–9954.

30 E. M. Jung, S. W. Lee and S. H. Kim, *Org. Electron.*, 2018, **52**, 123–129.

31 H. Lee, S. Lee, W. Lee, T. Yokota, K. Fukuda and T. Someya, *Adv. Funct. Mater.*, 2019, **29**, 1906982.

32 T. Someya, Z. Bao and G. G. Malliaras, *Nature*, 2016, **540**, 379–385.

33 P. C. Hutter, T. Rothlander, G. Scheipl and B. Stadlober, *IEEE Trans. Electron Devices*, 2015, **62**, 4231–4236.

34 C. G. Bischak, L. Q. Flagg and D. S. Ginger, *Adv. Mater.*, 2020, **32**, 2002610.

35 C. Qian, J. Sun, L. A. Kong, G. Gou, J. Yang, J. He, Y. Gao and Q. Wan, *ACS Appl. Mater. Interfaces*, 2016, **8**, 26169–26175.

36 L.-A. Kong, J. Sun, C. Qian, Y. Fu, J. Wang, J. Yang and Y. Gao, *Org. Electron.*, 2017, **47**, 126–132.

37 M. Petkovic, K. R. Seddon, L. P. Rebelo and C. S. Pereira, *Chem. Soc. Rev.*, 2011, **40**, 1383–1403.

38 Y. A. Yuen, L. Porcarelli, H. R. Aguirresarobe, A. Sanchez-Sanchez, I. Del Agua, U. Ismailov, G. G. Malliaras, D. Mecerreyes, E. Ismailova and H. Sardon, *Polymers*, 2018, **10**, 989.

39 W. Wang, Z. Li, M. Li, L. Fang, F. Chen, S. Han, L. Lan, J. Chen, Q. Chen, H. Wang, C. Liu, Y. Yang, W. Yue and Z. Xie, *Nano-Micro Lett.*, 2022, **14**, 184.

40 H. Yuk, B. Lu and X. Zhao, *Chem. Soc. Rev.*, 2019, **48**, 1642–1667.

41 X. Liu, J. Liu, S. Lin and X. Zhao, *Mater. Today*, 2020, **36**, 102–124.

42 Y. J. Jo, K. Y. Kwon, Z. U. Khan, X. Crispin and T. I. Kim, *ACS Appl. Mater. Interfaces*, 2018, **10**, 39083–39090.

43 J. Ko, X. Wu, A. Surendran, B. T. Muhammad and W. L. Leong, *ACS Appl. Mater. Interfaces*, 2020, **12**, 33979–33988.

44 S. Han, S. Yu, S. Hu, H.-J. Chen, J. Wu and C. Liu, *J. Mater. Chem. C*, 2021, **9**, 11801–11808.

45 S. Han, S. Yu, S. Hu, X. Liang, Y. Luo and C. Liu, *Org. Electron.*, 2022, **108**, 106605.

46 I. Cunha, J. Martins, D. Gaspar, P. G. Bahubalindruni, E. Fortunato, R. Martins and L. Pereira, *Adv. Electron. Mater.*, 2021, **7**, 2001166.

47 Z. Wu, X. Yang and J. Wu, *ACS Appl. Mater. Interfaces*, 2021, **13**, 2128–2144.

48 S. Peng, S. Liu, Y. Sun, N. Xiang, X. Jiang and L. Hou, *Eur. Polym. J.*, 2018, **106**, 206–213.

49 F. Yokoyama, I. Masada, K. Shimamura, T. Ikawa and K. Monobe, *Colloid Polym. Sci.*, 1986, **264**, 595–601.

50 J. E. Hagler, C. Kim, P. Kateb, J. Yeu, N. Gagnon-Lafrenais, E. Gee, S. Audry and F. Cicoira, *Flexible Printed Electron.*, 2022, **7**, 014008.

51 S. Zhang, E. Hubis, G. Tomasello, G. Soliveri, P. Kumar and F. Cicoira, *Chem. Mater.*, 2017, **29**, 3126–3132.

52 J. Chen, W. Huang, D. Zheng, Z. Xie, X. Zhuang, D. Zhao, Y. Chen, N. Su, H. Chen, R. M. Pankow, Z. Gao, J. Yu, X. Guo, Y. Cheng, J. Strzalka, X. Yu, T. J. Marks and A. Facchetti, *Nat. Mater.*, 2022, **21**, 564–571.

53 T. D. Nguyen, T. Q. Trung, Y. Lee and N.-E. Lee, *Adv. Eng. Mater.*, 2022, **24**, 2100918.

54 L. Zhao, L. Pan, Z. Cao and Q. Wang, *J. Phys. Chem. B*, 2016, **120**, 13112–13117.

55 C. Lu, C. Hu, C. L. Ritt, X. Hua, J. Sun, H. Xia, Y. Liu, D. W. Li, B. Ma, M. Elimelech and J. Qu, *J. Am. Chem. Soc.*, 2021, **143**, 14242–14252.

56 G.-T. Go, Y. Lee, D.-G. Seo, M. Pei, W. Lee, H. Yang and T.-W. Lee, *Adv. Intell. Syst.*, 2020, **2**, 2000012.

57 S. Yamamoto, A. G. Polyravas, S. Han and G. G. Malliaras, *Adv. Electron. Mater.*, 2022, **8**, 2101186.

58 F. Decataldo, F. Bonafe, F. Mariani, M. Serafini, M. Tessarolo, I. Gualandi, E. Scavetta and B. Fraboni, *Polymers*, 2022, **14**, 1022.

59 D. A. Bernards and G. G. Malliaras, *Adv. Funct. Mater.*, 2007, **17**, 3538–3544.

60 K. H. Seol, S. J. Lee, K. G. Cho, K. Hong and K. H. Lee, *J. Mater. Chem. C*, 2018, **6**, 10987–10993.

61 S. Zhang, Y. Li, G. Tomasello, M. Anthonisen, X. Li, M. Mazzeo, A. Genco, P. Grutter and F. Cicoira, *Adv. Electron. Mater.*, 2019, **5**, 1900191.

62 Y. Li, S. Zhang, X. Li, V. R. N. Unnava and F. Cicoira, *Flexible Printed Electron.*, 2019, **4**, 044004.

63 M. Lerond, A. Subramanian, W. G. Skene and F. Cicoira, *Frontiers in Physics*, 2021, **9**, 708914.

64 R. Morais, D. H. Vieira, C. Gaspar, L. Pereira, R. Martins and E. N. Alves, *Semicond. Sci. Technol.*, 2021, **36**, 125005.

65 M. Afonso, J. Morgado and L. Alcácer, *J. Appl. Phys.*, 2016, **120**, 165502.

66 D. Majak, J. Fan and M. Gupta, *Sens. Actuators, B*, 2019, **286**, 111–118.

67 J. Fan, C. Montemagno and M. Gupta, *Org. Electron.*, 2019, **73**, 122–129.